

# Dynamically Optimized Nonadiabatic Holonomic Quantum Computation

Hai Xu,<sup>1,2</sup> Wanchun Li,<sup>3</sup> Tao Chen,<sup>4,5,\*</sup> Kejin Wei,<sup>1,2</sup> and Chengxian Zhang<sup>1,2,†</sup>

<sup>1</sup>*School of Physical Science and Technology, Guangxi University, Nanning 530004, China*

<sup>2</sup>*Guangxi Key Laboratory for Relativistic Astrophysics,*

*School of Physical Science and Technology, Guangxi University, Nanning 530004, China*

<sup>3</sup>*School of Science, Guilin University of Aerospace Technology, No.2, Jinji Road, Guilin, 541004, China*

<sup>4</sup>*Key Laboratory of Atomic and Subatomic Structure and Quantum Control (Ministry of Education),  
School of Physics, South China Normal University, Guangzhou 510006, China*

<sup>5</sup>*Guangdong Provincial Key Laboratory of Quantum Engineering and Quantum Materials,  
Guangdong-Hong Kong Joint Laboratory of Quantum Matter,*

*Frontier Research Institute for Physics, South China Normal University, Guangzhou 510006, China*

(Dated: September 25, 2024)

Nonadiabatic holonomic quantum computation (NHQC) is one of the promising approaches to realizing fault-tolerant quantum computation. However, due to the imperfect control in the experimental environments, the holonomic gate still needs to be further improved. Here, we propose a dynamically optimized NHQC (OPNHQC) scheme based on dynamically corrected gate technique. The scheme is implemented by carefully designing a sequence of elementary pulses to fulfill cyclic evolution, while the dynamical phase is not accumulated. In this way, the constructed holonomic gate is immune to the error. It is found that our scheme can correct the  $X$  error up to fourth order. In addition, combining with the DFS encoding our scheme can be immune to both the  $X$  and  $Z$  errors. Therefore, our proposed scheme offers a prospective way to the realization of scalable fault-tolerant holonomic quantum computation.

## I. INTRODUCTION

Quantum computation has been shown to have capabilities on specific problems that are not available in classical computation. Robust control of the quantum gate is crucial for realizing fault-tolerant quantum computation [1, 2]. However, in the real physical implementation, the gate would suffer a lot of errors, resulting in gate infidelity. Over the past year, many methods have been put forward to mitigate this problem, such as composite pulse sequences [3–5], designing gates using geometric space curves [6–9], and time optimal control [10–12]. Among various methods, geometric quantum gate is a promising approach, due to it uses the global property of the geometric phase. It is believed that the geometric phase is only related to the evolution path during the evolution process, and is not related to the details such as the speed of evolution [13–16].

Early geometric phases were obtained based on non-degenerate as well as degenerate parameter spaces evolving through adiabatic cycles [13, 14]. In order to overcome the unfavorable limitation that adiabatic geometric phases need to evolve very slowly, the geometric phases were generalized to nonadiabatic cases [15, 16]. Meanwhile, nonadiabatic holonomic quantum computation (NHQC) [17–32] based on non-Abelian geometric (holonomic) phases and nonadiabatic evolution have been proposed. So far, the holonomic gates have been experimentally verified in various quantum systems, such as superconducting circuits [33–36], trapped ions [37], nuclear magnetic resonance [38–40], and nitrogen-vacancy centers in diamond [41–46]. However, due to the imperfect control in the experimental environments, the holonomic gate

still suffers from the  $X$  and  $Z$  errors, which are the two typical control errors [47, 48].

In order to address the challenge of complex error correction in NHQC schemes, many theoretical approaches have been developed, such as the composite schemes [40, 49], dynamical decoupling techniques [50–52], pulse optimization techniques [35, 53–56], and dynamically corrected gates [57–59]. However, in these previous studies, the enhancement of gate robustness in some of these schemes is typically achieved at the expense of gate evolution time or the necessity of specific waveform. It is therefore necessary to develop further simplified and highly robust NHQC protocols. Notably, with the guidance of the dynamical correction method [60–62], the so-called dynamically corrected NHQC (DCNHQC) scheme in Ref. [57] was able to suppress  $X$  errors up to fourth order. This scheme shows the great merit of the dynamical correction for improving the holonomic gates.

Here, we propose a new type of dynamically optimized NHQC (OPNHQC) scheme to realize robust holonomic gates based on dynamically corrected gate technique [63, 64]. The scheme is implemented by carefully designing the elementary pulses to fulfill cyclic evolution, while the dynamical phase is not accumulated. In this way, it can be immune to the  $X$  error. It is found that our scheme can also correct the  $X$  error up to fourth order, which is similar to the case for the DCNHQC scheme [57]. Meanwhile, the infidelity is only as half as that for the DCNHQC scheme. In addition, the numerical simulation results clearly show that the OPNHQC can not only greatly enhance the robustness for the conventional single-loop NHQC scheme [20, 21, 23], but can also outperform the DCNHQC scheme as well as the typical composite two-loop NHQC (TLNHQC) scheme [40, 49]. Furthermore, our scheme can be very compatible with the decoherence free subspace (DFS) encoding [65–67] technique. In this way, it is able to suppress  $X$  error and  $Z$  error at the same time. Thus,

\* Electronic address: chentamail@163.com

† Electronic address: cxzhang@gxu.edu.cn

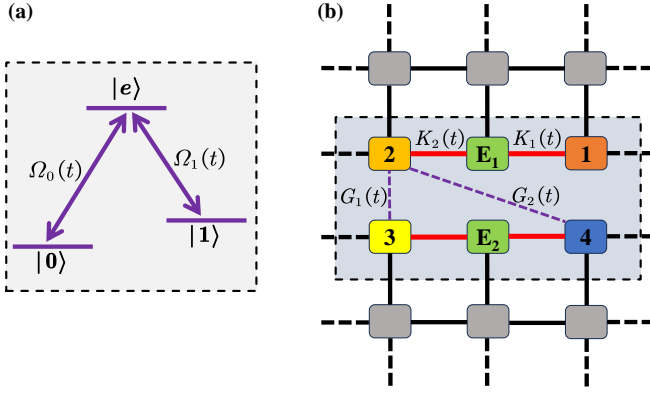


FIG. 1. (a) A general  $\Lambda$ -type three-level system with resonant transitions between  $|0\rangle \leftrightarrow |e\rangle$  and  $|1\rangle \leftrightarrow |e\rangle$ . (b) The coupling structure for realizing the DFS encoding implementation. Here, the physical qubits with different frequencies are represented by the (orange, gold, yellow and blue) colored squares. While the squares with green colors are regarded as the auxiliary physical qubits. Meanwhile, the interactions for single and two-qubit gates are denoted by the red solid and purple dashed lines, respectively.

our scheme can provide a promising strategy for large-scale fault-tolerant holonomic quantum computation.

## II. CONVENTIONAL HOLOMOMIC GATES

To begin with, we first introduce the realization of the conventional single-loop NHQC scheme [20, 21, 23], which is based on a general  $\Lambda$ -type three-level quantum system. As shown in Fig. 1(a), the system is resonantly driven by two different external pulses with the amplitudes  $\Omega_0(t)$  and  $\Omega_1(t)$ .  $\phi_0(t)$  and  $\phi_1(t)$  are the corresponding phases, respectively. Hereafter, we set  $\hbar = 1$ . Then, the Hamiltonian of the three-level system in the interaction picture is given by

$$\begin{aligned} \mathcal{H}(t) &= \left[ \Omega_0(t)e^{-i\phi_0(t)}|0\rangle + \Omega_1(t)e^{-i\phi_1(t)}|1\rangle \right] \langle e| + \text{H.c.} \\ &= \Omega(t)e^{-i\phi_0(t)}|b\rangle\langle e| + \text{H.c.} \end{aligned} \quad (1)$$

Here,  $\{|0\rangle, |1\rangle\}$  are the computational basis states,  $|e\rangle$  denotes the auxiliary state, and  $|b\rangle = \sin(\theta/2)|0\rangle - \cos(\theta/2)e^{i\phi}|1\rangle$  is the bright state with  $\phi = \phi_0 - \phi_1 + \pi$ . Except for the bright state,  $\mathcal{H}(t)$  also has a dark state  $|d\rangle = -\cos(\theta/2)e^{-i\phi}|0\rangle - \sin(\theta/2)|1\rangle$ , which is decoupled from the quantum dynamics. Note that, the amplitudes above have been parameterized as  $\Omega_0(t) = \Omega(t)\sin(\theta/2)$ ,  $\Omega_1(t) = \Omega(t)\cos(\theta/2)$ , and  $\Omega(t) = \sqrt{\Omega_0^2(t) + \Omega_1^2(t)}$ .

Then, based on the above Hamiltonian setting, the conventional single-loop NHQC scheme can be implemented by dividing the evolution into two segments

$$t \in [0, \tau_1], \quad \int_0^{\tau_1} \Omega(t)dt = \frac{\pi}{2}, \quad \phi_0(t) \equiv \phi'_0, \quad (2a)$$

$$t \in [\tau_1, \tau], \quad \int_{\tau_1}^{\tau} \Omega(t)dt = \frac{\pi}{2}, \quad \phi_0(t) \equiv \phi'_0 + \pi - \gamma_g. \quad (2b)$$

For these two segments, the corresponding evolution operators are thus  $U_1 = \exp(-i \int_0^{\tau_1} \mathcal{H}(t)dt)$  and  $U_2 = \exp(-i \int_{\tau_1}^{\tau} \mathcal{H}(t)dt)$ . As shown in Fig. 2(a), during the first half of the evolution, the evolution starts from the north pole and travels to the south pole along a given longitude. At the end of the evolution, it goes back to the north pole along another longitude ( $\gamma_g$  away from the original one) to finish the cyclic evolution. Finally,  $|b\rangle$  acquires a pure geometric phase  $\gamma_g$ . Meanwhile, during the whole process, the dark state  $|d\rangle$  does not change, because it always decouples from the dynamics. Then, in the dressed states basis spanned by  $\{|b\rangle, |d\rangle\}$ , the holonomic gate is thus

$$U = U_2 U_1 = |d\rangle\langle d| + e^{i\gamma_g}|b\rangle\langle b|. \quad (3)$$

On the other hand, one can easily turn the holonomic gate into the computational basis spanned by  $\{|0\rangle, |1\rangle\}$

$$\begin{aligned} U(\theta, \phi, \gamma_g) &= e^{i\frac{\gamma_g}{2}} \begin{pmatrix} \cos \frac{\gamma_g}{2} - i \sin \frac{\gamma_g}{2} \cos \theta & -i \sin \frac{\gamma_g}{2} \sin \theta e^{-i\phi} \\ -i \sin \frac{\gamma_g}{2} \sin \theta e^{i\phi} & \cos \frac{\gamma_g}{2} + i \sin \frac{\gamma_g}{2} \cos \theta \end{pmatrix} \\ &= e^{i\frac{\gamma_g}{2}} e^{-i\frac{\gamma_g}{2} \mathbf{n} \cdot \boldsymbol{\sigma}}, \end{aligned} \quad (4)$$

where  $\mathbf{n} = (\sin \theta \cos \phi, \sin \theta \sin \phi, \cos \theta)$ , and  $\boldsymbol{\sigma} = (\sigma_x, \sigma_y, \sigma_z)$  with  $\sigma_{x,y,z}$  representing the Pauli matrices in the computational basis. Then, by appropriately modulating the axis  $\mathbf{n}$  and the phase  $\gamma_g$ , one can realize arbitrary single-qubit holonomic quantum gate.

Meanwhile, in the presence of the  $X$  error, the Hamiltonian turns to be  $\mathcal{H}^\epsilon(t) = (1 + \epsilon)\mathcal{H}(t)$ . In this work, we treat  $\epsilon$  as an unknown constant value considering  $|\epsilon| \ll 1$ . In this way it can be regarded as the perturbation term. This is always reasonable for the state-of-the-art platforms, such as superconducting circuit [68], Rydberg atoms [69]. Thus, the evolution operator with error is expressed as  $U_{\text{con}}^\epsilon(t) = e^{-i \int \mathcal{H}^\epsilon(t)dt}$ . In the dressed state basis  $\{|b\rangle, |d\rangle\}$ , it has the form as

$$U_{\text{con}}^\epsilon = |d\rangle\langle d| + \left( \cos^2 \frac{\mu\pi}{2} + \sin^2 \frac{\mu\pi}{2} e^{i\gamma_g} \right) |b\rangle\langle b|, \quad (5)$$

where  $\mu = 1 + \epsilon$ . With this error operator, we can further expand its fidelity as

$$\begin{aligned} F_{\text{con}} &= \frac{1}{2} \left| 1 + \cos^2 \frac{\mu\pi}{2} e^{-i\gamma_g} + \sin^2 \frac{\mu\pi}{2} \right| \\ &\approx 1 - \epsilon^2 \pi^2 (1 - \cos \gamma_g) / 8, \end{aligned} \quad (6)$$

where the fidelity [57, 70] is defined as

$$F = \frac{|\text{Tr}(U^\dagger U^\epsilon)|}{|\text{Tr}(U^\dagger U)|}. \quad (7)$$

It is clear that the conventional holonomic gate is immune to the leading order error. In other words, it can only suppress the  $X$  error to the second order. Similarly, another typical holonomic gate, i.e., the TLNHQC scheme [40, 49] can suppress the  $X$  error to the same level (see Eq. (A3) in Appendix. A).

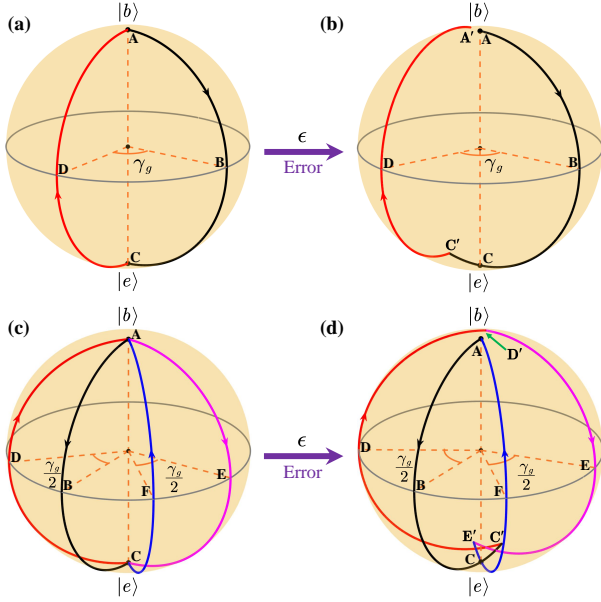


FIG. 2. The evolution trajectories for holonomic quantum gates in Eqs. (4) and (9) with  $\gamma_g = \pi/2$ . Without considering the  $X$  error, the trajectories in (a) and (c) denote the evolution path for the conventional NHQC and OPNHQC schemes, respectively. In (a), the trajectory is along  $A \rightarrow B \rightarrow C \rightarrow D \rightarrow A$ , while in (c), it is along  $A \rightarrow B \rightarrow C \rightarrow D \rightarrow A \rightarrow E \rightarrow C \rightarrow F \rightarrow A$ . (b) and (d) are the corresponding cases for (a) and (c), respectively, considering the presence of  $X$  error. In (b), the trajectory is along  $A \rightarrow B \rightarrow C \rightarrow C' \rightarrow D \rightarrow A'$ , and (d) along  $A \rightarrow B \rightarrow C \rightarrow C' \rightarrow D \rightarrow D' \rightarrow E \rightarrow E' \rightarrow F \rightarrow A$ .

### III. DYNAMICALLY OPTIMIZED HOLONOMIC GATES

As stated above, the conventional holonomic gate implemented in the single-loop way is easily sensitive to the  $X$  error. As all we know that, in the presence of the  $X$  error, it would bring about unwanted over-rotation problem. For the conventional single-loop NHQC scheme as shown in Fig. 1(b), the state would deviate from the south pole when  $t = \tau_1$ , and cannot exactly return back to the initial north pole to fulfill cyclic evolution at the final time  $\tau$ . To circumvent this problem, we introduce the OPNHQC scheme based on dynamically corrected gates technique. The central idea for the dynamically corrected gate is that a naive pulse can be replaced by a sequence of elementary pulses [63, 64]. On the one hand, these two set of pulses are equivalent. On the other hand, the noise concerned is self-compensated and eliminated during the evolution process. Here, our strategy is to construct a robust composite sequence, where its evolution operator  $U'_2$  is equivalent to  $U_2$ . To do this, we implement it by carefully designing a three-elementary pulses. Meanwhile, we do not change the first evolution in Eq. (2). Such that the  $X$  error in the total evolution  $U'_2 U_1$  is self-compensated. On the other hand, it is needed to make sure that the pulses would not introduce external dynamical phase. As shown in Fig. 2(c), we plot the evolution process for the OPNHQC scheme without con-

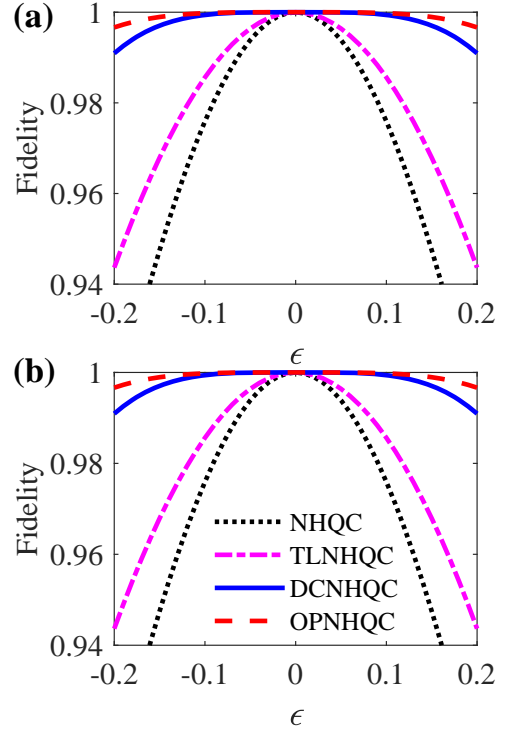


FIG. 3. Robustness of the OPNHQC scheme compared to the NHQC, TLNHQC, DCNHQC schemes, where (a) denotes  $X/2$  and (b) the  $S$  gate. The decoherence rate is set to be zero.

sidering the error effect. While in Fig. 1(d), the evolution can still fulfill cyclic evolution even in the presence of the  $X$  error. Then, the corresponding Hamiltonian and control parameters satisfy the following form

$$t \in [0, \tau'_1], \int_0^{\tau'_1} \Omega(t) dt = \frac{\pi}{2}, \quad \phi_0(t) \equiv \phi'_0, \quad (8a)$$

$$t \in [\tau'_1, \tau'_2], \int_{\tau'_1}^{\tau'_2} \Omega(t) dt = \frac{\pi}{2}, \quad \phi_0(t) \equiv \phi'_0 + \pi - \frac{\gamma_g}{2}, \quad (8b)$$

$$t \in [\tau'_2, \tau'_3], \int_{\tau'_2}^{\tau'_3} \Omega(t) dt = \frac{\pi}{2}, \quad \phi_0(t) \equiv \phi'_0 + \pi - \gamma_g, \quad (8c)$$

$$t \in [\tau'_3, \tau'], \int_{\tau'_3}^{\tau'} \Omega(t) dt = \frac{\pi}{2}, \quad \phi_0(t) \equiv \phi'_0 + 2\pi - \frac{3\gamma_g}{2}, \quad (8d)$$

where the posterior three-elementary pulses in Eq. 8(b)-(d) corresponds to the operator  $U'_2 = \exp(-i \int_{\tau'_1}^{\tau'} \mathcal{H}(t) dt)$ . Based on the above settings, the final holonomic gate in the computational basis of  $\{|0\rangle, |1\rangle\}$  is

$$U = U'_2 U_1 = e^{i\frac{\gamma_g}{2}} e^{-i\frac{\gamma_g}{2} \mathbf{n} \cdot \boldsymbol{\sigma}}, \quad (9)$$

which has the same form in Eq. (4). Thus, we can use this scheme to realize universal holonomic gates. It is worth men-

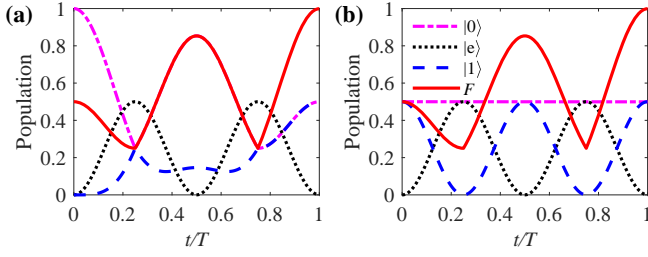


FIG. 4. The state population and fidelity dynamics of (a)  $X/2$  and (b)  $S$  gates for the OPNHQC scheme. The decoherence rates are chosen as a moderate value  $\Gamma = 2 \times 10^{-4}$

tioning that although we insert the composite pulses, the dynamical phase is not accumulated during the whole evolution, since the evolution trajectory is always along the longitude [53].

On the other hand, when the  $X$  error is present, the operator for the OPNHQC scheme in the dressed states basis  $\{|b\rangle, |d\rangle\}$  will change from the ideal case to

$$U_{\text{op}}^{\epsilon} = |d\rangle\langle d| + \left[ e^{i\gamma_g} - 2ie^{i\gamma_g} \sin \frac{\gamma_g}{2} \left( \cos^4 \frac{\mu\pi}{2} e^{-i\frac{\gamma_g}{2}} + \frac{1}{4} \sin^2 \mu\pi \right) \right] |b\rangle\langle b|. \quad (10)$$

The gate fidelity can then be expanded as

$$F_{\text{op}} = \frac{1}{2} \left| 2 - 2i \sin \frac{\gamma_g}{2} \left( \cos^4 \frac{\mu\pi}{2} e^{-i\frac{\gamma_g}{2}} + \frac{1}{4} \sin^2 \mu\pi \right) \right| \approx 1 - \epsilon^4 \pi^4 (1 - \cos \gamma_g) / 64. \quad (11)$$

It is clear that our OPNHQC scheme can improve the conventional NHQC against the  $X$  error from second to the fourth order. Meanwhile, the OPNHQC scheme can still outperform the DCNHQC scheme [57], which can also suppress the error to the fourth order (see Appendix. B). This can be verified by comparing the infidelity performance between Eq. (11) and Eq. (B3), where the infidelity for the former is only half as that for the later. In Fig. (3), we take the  $X/2$  and  $S$  gates as two typical examples to verify the excellent robustness performance for our OPNHQC scheme. The parameters for these two gates are  $\{\theta = \pi/2, \gamma_g = \pi/2, \phi = 0\}$ , and  $\{\theta = 0, \gamma_g = \pi/2, \phi = 0\}$ , respectively. In both cases, it can outperform all the counterparts.

### A. The gate performance

Here, we consider a general  $\Lambda$ -type three-level quantum system to faithfully demonstrate the superiority of the OPNHQC scheme. The gate performance is evaluated by using the Lindblad master equation

$$\dot{\rho}_0 = i[\rho_0, \mathcal{H}] + \frac{1}{2} \sum_{j=1}^4 \Gamma_j \mathcal{L}(\sigma_j), \quad (12)$$

where  $\rho_0$  is the density matrix of the considered system and  $\mathcal{L}(\sigma_j) = 2\sigma_j \rho_0 \sigma_j^\dagger - \sigma_j^\dagger \sigma_j \rho_0 - \rho_0 \sigma_j^\dagger \sigma_j$  represents the Lindbladian of the operator  $\sigma_j$  with  $\sigma_1 = |e\rangle\langle 0|$ ,  $\sigma_2 = |e\rangle\langle 1|$ ,  $\sigma_3 = (|0\rangle\langle 0| - |e\rangle\langle e|)/2$ ,  $\sigma_4 = (|1\rangle\langle 1| - |e\rangle\langle e|)/2$ , and  $\Gamma_j$  are the corresponding decoherence rate. When considering the current state-of-the-art technologies, the ratio of  $\Gamma_j/\Omega_m$  can be as low as  $\sim 10^{-4}$ , where  $\Omega_m$  denotes the maximum value of  $\Omega(t)$ . For simplicity, we set  $\Omega(t) = \Omega_m = 1$  and  $\phi'_0 = 0$  to simulate the performance of our OPNHQC scheme with and without considering the  $X$  error.

We first verify the state population and state fidelity without considering the  $X$  error. Here, we give two gates as examples, namely  $X/2$  and  $S$  gates. The initial states are set to be  $|\psi_i\rangle_{X/2} = |0\rangle$  and  $|\psi_i\rangle_S = (|0\rangle + |1\rangle)/\sqrt{2}$ . The state fidelity is defined as  $F_{X/2(S)} = \langle \psi_f | \rho_0 | \psi_f \rangle_{X/2(S)}$  to evaluate these two holonomic gates. And the corresponding ideal target states are  $|\psi_f\rangle_{X/2} = (|0\rangle + |1\rangle)/2 + i(|0\rangle - |1\rangle)/2$  and  $|\psi_f\rangle_S = (|0\rangle + i|1\rangle)/\sqrt{2}$ . Here, the decoherence rates are chosen as a moderate value  $\Gamma_1 = \Gamma_2 = \Gamma_3 = \Gamma_4 = \Gamma = 2 \times 10^{-4}$ . As shown in Figs. 4(a) and (b), we obtain the state fidelities for the  $X/2$  and  $S$  gate as  $F_{X/2} = 99.90\%$  and  $F_S = 99.89\%$ , respectively. Then, to fully evaluate the average gate performance, we consider using six typical initial states as  $\{|0\rangle, |1\rangle, (|0\rangle - |1\rangle)/\sqrt{2}, (|0\rangle + |1\rangle)/\sqrt{2}, (|0\rangle - i|1\rangle)/\sqrt{2}, (|0\rangle + i|1\rangle)/\sqrt{2}\}$ , and the corresponding gate fidelity is defined as [71–73]

$$F_1^G = \frac{1}{6} \sum_{k=1}^6 \langle \psi_i | U^\dagger \rho_0 U | \psi_i \rangle_k. \quad (13)$$

It is found that the average fidelities for the two gates are  $F_{X/2}^G = 99.89\%$  and  $F_S^G = 99.90\%$ , respectively. Furthermore, the numerical results confirm that when  $\Gamma < 2 \times 10^{-4}$ , the fidelities for both gates can exceed 99.90%.

Then, we demonstrate the robustness of our dynamically optimized holonomic gates considering both the  $X$  error and decoherence effect. As shown in Fig. (5), the decoherence rate is with  $\Gamma_j = \Gamma \in [0, 5] \times 10^{-4}$  and the error is within the range of  $-0.1 \leq \epsilon \leq 0.1$ . It is clear that both the OPNHQC in (d) and DCNHQC [57] in (c) can substantially improve the gate robustness for the  $X/2$  gate, compared to the conventional single-loop NHQC [23] in (a) and composite TLNHQC [40, 49] in (b). In addition, from Figs. 5(c) and (d), within all the range of  $-0.1 \leq \epsilon \leq 0.1$ , the fidelity for the DCNHQC scheme can be higher than 99.9% when  $\Gamma \leq 0.8 \times 10^{-4}$ . While for our OPNHQC protocol, the gate fidelity can be higher than 99.9% when  $\Gamma \leq 1.4 \times 10^{-4}$ . This result indicates superior gate robustness of our protocol.

## IV. PHYSICAL IMPLEMENTATION

As stated above, the OPNHQC scheme can effectively suppress the  $X$  error. Below we show that our scheme can be very compatible with the DFS encoding technique [65–67] so as to synchronously suppress the  $X$  and  $Z$  errors. As shown in Fig. 1(b), for the DFS encoding scheme, the logical qubit



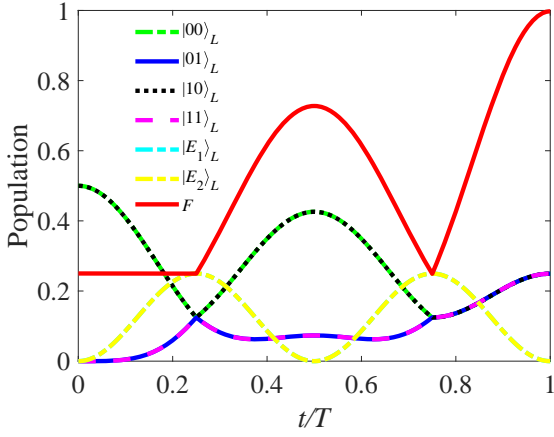


FIG. 7. State dynamics of the two-qubit gate  $U'_T$ . The initial state is set to be  $(|00\rangle_L + |10\rangle_L)/\sqrt{2}$ , and the decoherence rate is  $\Gamma = 2 \times 10^{-4}$ .

Here, benefiting from the subspace  $\text{Span}\{|00\rangle_L, |01\rangle_L, |E_1\rangle_L\}$  and  $\text{Span}\{|10\rangle_L, |11\rangle_L, |E_2\rangle_L\}$ , there are two block-diagonal three-level structures that can be used to construct nontrivial two-qubit holonomic gates, which can suppresses both the  $X$  and  $Z$  errors. When satisfying  $\int_0^\tau \sqrt{G_1(t)^2 + G_2(t)^2} dt = 2\pi$ , the Hamiltonian in Eq. (18) leads to an evolution operator as

$$U_T(\chi, \eta, \gamma_g) = \begin{pmatrix} \alpha e^{-i\frac{\gamma_g}{2}} & i\beta^* e^{-i\frac{\gamma_g}{2}} & 0 & 0 & 0 & 0 \\ i\beta e^{-i\frac{\gamma_g}{2}} & \alpha^* e^{-i\frac{\gamma_g}{2}} & 0 & 0 & 0 & 0 \\ 0 & 0 & e^{i\gamma_g} & 0 & 0 & 0 \\ 0 & 0 & 0 & \alpha e^{i\frac{\gamma_g}{2}} & -i\beta^* e^{i\frac{\gamma_g}{2}} & 0 \\ 0 & 0 & 0 & -i\beta e^{i\frac{\gamma_g}{2}} & \alpha^* e^{i\frac{\gamma_g}{2}} & 0 \\ 0 & 0 & 0 & 0 & 0 & e^{-i\gamma_g} \end{pmatrix}, \quad (19)$$

where  $\tan(\chi/2) = G_1(t)/G_2(t)$ , and  $\eta = \eta_3 - \eta_4 + \pi$ . In addition,  $\alpha$  and  $\beta$  satisfy  $\alpha \equiv \cos(\gamma_g/2) + i \cos \chi \sin(\gamma_g/2)$ , and  $\beta \equiv \sin \chi \sin(\gamma_g/2) e^{-i\eta}$ . Then, we can use the operator  $U_T(\chi, \eta, \gamma_g)$  to realize nontrivial two-qubit gates.

Notably, since  $U_T(\chi, \eta, \gamma_g)$  is block diagonalized, there is no transition between the logical-qubit subspace  $\text{Span}\{|00\rangle_L, |01\rangle_L, |10\rangle_L, |11\rangle_L\}$  and the auxiliary subspace  $\text{Span}\{|E_1\rangle_L, |E_2\rangle_L\}$ . Then, the evolution operator in the logical-qubit subspace can be reduced as

$$U'_T(\chi, \eta, \gamma_g) = \begin{pmatrix} \alpha e^{-i\frac{\gamma_g}{2}} & i\beta^* e^{-i\frac{\gamma_g}{2}} & 0 & 0 \\ i\beta e^{-i\frac{\gamma_g}{2}} & \alpha^* e^{-i\frac{\gamma_g}{2}} & 0 & 0 \\ 0 & 0 & \alpha e^{i\frac{\gamma_g}{2}} & -i\beta^* e^{i\frac{\gamma_g}{2}} \\ 0 & 0 & -i\beta e^{i\frac{\gamma_g}{2}} & \alpha^* e^{i\frac{\gamma_g}{2}} \end{pmatrix}. \quad (20)$$

Thus, by setting  $\chi = \pi/2$ ,  $\eta = 0$ , and  $\gamma_g = \pi/2$ , we can get a nontrivial two-qubit gate, i.e.,  $U'_T(\pi/2, 0, \pi/2)$ , which is equivalent to the CNOT gate up to a local single-qubit gate

operation for the second logical qubit [78–80] as

$$U'_T \times (I_1 \otimes (X/2)_2) = \begin{pmatrix} 1 & 0 & 0 & 0 \\ 0 & 1 & 0 & 0 \\ 0 & 0 & 0 & 1 \\ 0 & 0 & 1 & 0 \end{pmatrix} = \text{CNOT}. \quad (21)$$

As shown in Fig. 7, we show the state fidelity for the constructed two-qubit gate  $U'_T$ . Here, we consider the initial state as  $(|00\rangle_L + |10\rangle_L)/\sqrt{2}$  and the decoherence rate as  $\Gamma = 2 \times 10^{-4}$ . The state fidelity can reach 99.74%. The gate infidelity here is mainly owing to the qubit decay effect. It is noteworthy that our two-qubit holonomic gates with DFS encoding are also capable of effectively resisting the  $Z$  error caused by collective dephasing.

## V. CONCLUSION

In conclusion, we propose a dynamically optimized NHQC scheme to improve the holonomic gate performance. Based on the dynamically corrected gate technique, the OPNHQC scheme can suppress the  $X$  error up to fourth order. In particular, combining with the DFS encoding our scheme can be immune to both the  $X$  and  $Z$  errors. Compared with the previous implementations, the numerical simulation results show that our current OPNHQC strategy achieves very excellent performance. Therefore, our scheme is promising for future scalable fault-tolerant holonomic quantum computation.

## ACKNOWLEDGMENTS

This work was supported by the National Natural Science Foundation of China (Grant No. 11905065, 62171144, 12305019), the Guangxi Science Foundation (Grant No. AD22035186, 2021GXNSFAA220011) and the Project of Improving the Basic Scientific Research Ability of Young and Middle-aged Teachers in Universities of Guangxi (Grant No. 2023KY0815).

## Appendix A: The TLNHQC Scheme

Below we discuss how to use the composite two-loop NHQC to construct the TLNHQC Scheme [40, 49]. Based on the composite pulse technology, the conventional NHQC scheme in Eq. (2) can be extended to the composite holonomic gate form. The evolution operation has the relation:  $[U(\theta, \phi, \gamma_g/N)]^N = U(\theta, \phi, \gamma_g)$ ,  $N$  is the number of composite pulse. Here we just consider the case of  $N = 2$ . The control parameters of the composite two-loop NHQC scheme

are given by

$$\begin{aligned}
t \in [0, T/2], \int_0^{T/2} \Omega(t) dt &= \frac{\pi}{2}, & \phi_0 &\equiv \phi'_0, \\
t \in \left[\frac{T}{2}, T\right], \int_{\frac{T}{2}}^T \Omega(t) dt &= \frac{\pi}{2}, & \phi_0 &\equiv \phi'_0 + \pi - \frac{\gamma_g}{2}, \\
t \in \left[T, \frac{3T}{2}\right], \int_T^{\frac{3T}{2}} \Omega(t) dt &= \frac{\pi}{2}, & \phi_0 &\equiv \phi'_0, \\
t \in \left[\frac{3T}{2}, 2T\right], \int_{\frac{3T}{2}}^{2T} \Omega(t) dt &= \frac{\pi}{2}, & \phi_0 &\equiv \phi'_0 + \pi - \frac{\gamma_g}{2}.
\end{aligned} \tag{A1}$$

For this case, the total gate-time will be  $2T$  and the total pulse area is  $2\pi$ . The final evolution has the same form as shown in Eq. (4). When the holonomic gates suffer from the influence of  $X$  error, the operation in the dressed basis  $\{|b\rangle, |d\rangle\}$  can be expressed as

$$\begin{aligned}
U_{tl}^\epsilon &= |d\rangle\langle d| + \left[ \sin^2 \mu\pi \left( \cos \frac{\gamma_g}{2} + e^{i\frac{\gamma_g}{2}} \right) / 2 \right. \\
&\quad \left. + \sin^4 \mu\pi e^{i\gamma_g} + \cos^2 \frac{\mu\pi}{2} \left( 1 - 3 \sin^2 \frac{\mu\pi}{2} \right) \right] |b\rangle\langle b|.
\end{aligned} \tag{A2}$$

For the TLNHQC scheme, the gate fidelity can be expanded as

$$\begin{aligned}
F_{tl} &= \frac{1}{2} \left| 1 + \frac{1}{2} \sin^2 \mu\pi \left( \cos \frac{\gamma_g}{2} + e^{i\frac{\gamma_g}{2}} \right) e^{-i\gamma_g} + \sin^4 \frac{\mu\pi}{2} \right. \\
&\quad \left. + \cos^2 \frac{\mu\pi}{2} \left( 1 - 3 \sin^2 \frac{\mu\pi}{2} \right) e^{-i\gamma_g} \right| \\
&\approx 1 - \epsilon^2 \pi^2 \sin^2 \frac{\gamma_g}{4} \cos^2 \frac{\gamma_g}{2}.
\end{aligned} \tag{A3}$$

## Appendix B: The DCNHQC Scheme

With the guidance of the dynamical correction method [60–62], the work in Ref. [57] was able to suppress  $X$  errors up to fourth order by inserting two pulses at the middle point in

each half of the evolution path in the conventional NHQC. Accordingly, the control parameters in the Hamiltonian can be

$$\begin{aligned}
t \in [0, T/4], \int_0^{T/4} \Omega(t) dt &= \frac{\pi}{4}, & \phi_0 &\equiv \phi'_0, \\
t \in \left[\frac{T}{4}, \frac{3T}{4}\right], \int_{\frac{T}{4}}^{\frac{3T}{4}} \Omega(t) dt &= \frac{\pi}{2}, & \phi_0 &\equiv \phi'_0 + \frac{\pi}{2}, \\
t \in \left[\frac{3T}{4}, T\right], \int_{\frac{3T}{4}}^T \Omega(t) dt &= \frac{\pi}{4}, & \phi_0 &\equiv \phi'_0, \\
t \in \left[T, \frac{5T}{4}\right], \int_T^{\frac{5T}{4}} \Omega(t) dt &= \frac{\pi}{4}, & \phi_0 &\equiv \phi'_0 + \pi - \gamma_g, \\
t \in \left[\frac{5T}{4}, \frac{7T}{4}\right], \int_{\frac{5T}{4}}^{\frac{7T}{4}} \Omega(t) dt &= \frac{\pi}{2}, & \phi_0 &\equiv \phi'_0 - \frac{\pi}{2} - \gamma_g, \\
t \in \left[\frac{7T}{4}, 2T\right], \int_{\frac{7T}{4}}^{2T} \Omega(t) dt &= \frac{\pi}{4}, & \phi_0 &\equiv \phi'_0 + \pi - \gamma_g.
\end{aligned} \tag{B1}$$

Notably, the whole process can still realize universal single-qubit holonomic gates, as the same in Eq. (4). And the total pulse area is also  $2\pi$ . When the  $X$  error is taken into account, the holonomic gates in the dressed basis  $\{|b\rangle, |d\rangle\}$  will change to

$$\begin{aligned}
U_{dc}^\epsilon &= \left[ \cos^4 \frac{\mu\pi}{2} + \left( \sin^2 \frac{\mu\pi}{2} + \frac{1}{4} \sin^2 \mu\pi \right) e^{i\gamma_g} \right] |b\rangle\langle b| \\
&\quad + |d\rangle\langle d|.
\end{aligned} \tag{B2}$$

For the DCNHQC scheme, the gate fidelity can be expanded as

$$\begin{aligned}
F_{dc} &= \frac{1}{2} \left| 1 + \sin^2 \frac{\mu\pi}{2} + \frac{1}{4} \sin^2 \mu\pi + \cos^4 \frac{\mu\pi}{2} e^{-i\gamma_g} \right| \\
&\approx 1 - \epsilon^4 \pi^4 (1 - \cos \gamma_g) / 32.
\end{aligned} \tag{B3}$$

- 
- [1] J. Preskill, Quantum computing in the NISQ era and beyond, *Quantum* **2**, 79 (2018).
- [2] K. Bharti, A. Cervera-Lierta, T. H. Kyaw, T. Haug, S. Alperin-Lea, A. Anand, M. Degroote, H. Heimonen, J. S. Kottmann, T. Menke, W.-K. Mok, S. Sim, L.-C. Kwek, and A. Aspuru-Guzik, Noisy intermediate-scale quantum algorithms, *Rev. Mod. Phys.* **94**, 015004 (2022).
- [3] Y. Ota and Y. Kondo, Composite pulses in NMR as non-adiabatic geometric quantum gates, *Phys. Rev. A* **80**, 024302 (2009).
- [4] B. T. Torosov and N. V. Vitanov, High-fidelity error-resilient composite phase gates, *Phys. Rev. A* **90**, 012341 (2014).
- [5] H. L. Gevorgyan and N. V. Vitanov, Ultrahigh-fidelity composite rotational quantum gates, *Phys. Rev. A* **104**, 012609 (2021).
- [6] W. Dong, F. Zhuang, S. E. Economou, and E. Barnes, Doubly Geometric Quantum Control, *PRX Quantum* **2**, 030333 (2021).
- [7] E. Barnes, F. A. Calderon-Vargas, W. Dong, B. Li, J. Zeng, and F. Zhuang, Dynamically corrected gates from geometric space curves, *Quantum Sci. Technol.* **7**, 023001 (2022).
- [8] H. L. Tang, K. Connelly, A. Warren, F. Zhuang, S. E. Economou, and E. Barnes, Designing Globally Time-Optimal Entangling Gates Using Geometric Space Curves, *Phys. Rev. Appl.* **19**, 044094 (2023).
- [9] H. T. Nelson, E. Piliouras, K. Connelly, and E. Barnes, Designing dynamically corrected gates robust to multiple noise sources using geometric space curves, *Phys. Rev. A* **108**, 012407 (2023).
- [10] A. Carlini and T. Koike, Time-optimal transfer of coherence, *Phys. Rev. A* **86**, 054302 (2012).
- [11] J. Geng, Y. Wu, X. Wang, K. Xu, F. Shi, Y. Xie, X. Rong, and J. Du, Experimental Time-Optimal Universal Control of Spin Qubits in Solids, *Phys. Rev. Lett.* **117**, 170501 (2016).

- [12] Y. Dong, C. Feng, Y. Zheng, X.-D. Chen, G.-C. Guo, and F.-W. Sun, Fast high-fidelity geometric quantum control with quantum brachistochrones, *Phys. Rev. Res.* **3**, 043177 (2021).
- [13] M. V. Berry, Quantal phase factors accompanying adiabatic changes, *Proc. R. Soc. London A* **392**, 45 (1984).
- [14] F. Wilczek and A. Zee, Appearance of Gauge Structure in Simple Dynamical Systems, *Phys. Rev. Lett.* **52**, 2111 (1984).
- [15] Y. Aharonov and J. Anandan, Phase change during a cyclic quantum evolution, *Phys. Rev. Lett.* **58**, 1593 (1987).
- [16] J. Anandan, Non-adiabatic non-abelian geometric phase, *Phys. Lett. A* **133**, 171 (1988).
- [17] P. Zanardi and M. Rasetti, Holonomic quantum computation, *Phys. Lett. A* **264**, 94 (1999).
- [18] E. Sjöqvist, D. M. Tong, L. M. Andersson, B. Hessmo, M. Johansson, and K. Singh, Non-adiabatic holonomic quantum computation, *New J. Phys.* **14**, 103035 (2012).
- [19] G. F. Xu, J. Zhang, D. M. Tong, E. Sjöqvist, and L. C. Kwek, Nonadiabatic Holonomic Quantum Computation in Decoherence-Free Subspaces, *Phys. Rev. Lett.* **109**, 170501 (2012).
- [20] G. F. Xu, C. L. Liu, P. Z. Zhao, and D. M. Tong, Nonadiabatic holonomic gates realized by a single-shot implementation, *Phys. Rev. A* **92**, 052302 (2015).
- [21] E. Herterich and E. Sjöqvist, Single-loop multiple-pulse nonadiabatic holonomic quantum gates, *Phys. Rev. A* **94**, 052310 (2016).
- [22] B.-J. Liu, Z.-H. Huang, Z.-Y. Xue, and X.-D. Zhang, Superadiabatic holonomic quantum computation in cavity QED, *Phys. Rev. A* **95**, 062308 (2017).
- [23] Z.-P. Hong, B.-J. Liu, J.-Q. Cai, X.-D. Zhang, Y. Hu, Z. D. Wang, and Z.-Y. Xue, Implementing universal nonadiabatic holonomic quantum gates with transmons, *Phys. Rev. A* **97**, 022332 (2018).
- [24] P. Z. Zhao, K. Z. Li, G. F. Xu, and D. M. Tong, General approach for constructing Hamiltonians for nonadiabatic holonomic quantum computation, *Phys. Rev. A* **101**, 062306 (2020).
- [25] B.-J. Liu and M.-H. Yung, Leakage Suppression for Holonomic Quantum Gates, *Phys. Rev. Appl.* **14**, 034003 (2020).
- [26] L.-N. Ji, Y. Liang, P. Shen, and Z.-Y. Xue, Nonadiabatic Holonomic Quantum Computation via Path Optimization, *Phys. Rev. Appl.* **18**, 044034 (2022).
- [27] Y. Liang, P. Shen, T. Chen, and Z.-Y. Xue, Composite Short-Path Nonadiabatic Holonomic Quantum Gates, *Phys. Rev. Appl.* **17**, 034015 (2022).
- [28] B.-J. Liu, L.-L. Yan, Y. Zhang, M.-H. Yung, S.-L. Su, and C. X. Shan, Decoherence-suppressed nonadiabatic holonomic quantum computation, *Phys. Rev. Res.* **5**, 013059 (2023).
- [29] P. Z. Zhao and D. M. Tong, Nonadiabatic holonomic quantum computation based on a commutation relation, *Phys. Rev. A* **108**, 012619 (2023).
- [30] X.-D. Yu and D. M. Tong, Evolution Operator Can Always Be Separated into the Product of Holonomy and Dynamic Operators, *Phys. Rev. Lett.* **131**, 200202 (2023).
- [31] J. Zhang, T. H. Kyaw, S. Filipp, L.-C. Kwek, E. Sjöqvist, and D. Tong, Geometric and holonomic quantum computation, *Phys. Rep.* **1027**, 1 (2023).
- [32] Y. Liang, P. Shen, T. Chen, and Z.-Y. Xue, Nonadiabatic holonomic quantum computation and its optimal control, *Sci. China Inf. Sci.* **66**, 180502 (2023).
- [33] A. A. Abdumalikov Jr, J. M. Fink, K. Juliusson, M. Pechal, S. Berger, A. Wallraff, and S. Filipp, Experimental realization of non-Abelian non-adiabatic geometric gates, *Nature* **496**, 482 (2013).
- [34] Y. Xu, W. Cai, Y. Ma, X. Mu, L. Hu, T. Chen, H. Wang, Y. P. Song, Z.-Y. Xue, Z.-q. Yin, and L. Sun, Single-Loop Realization of Arbitrary Nonadiabatic Holonomic Single-Qubit Quantum Gates in a Superconducting Circuit, *Phys. Rev. Lett.* **121**, 110501 (2018).
- [35] T. Yan, B.-J. Liu, K. Xu, C. Song, S. Liu, Z. Zhang, H. Deng, Z. Yan, H. Rong, K. Huang, M.-H. Yung, Y. Chen, and D. Yu, Experimental Realization of Nonadiabatic Shortcut to Non-Abelian Geometric Gates, *Phys. Rev. Lett.* **122**, 080501 (2019).
- [36] S. Li, B.-J. Liu, Z. Ni, L. Zhang, Z.-Y. Xue, J. Li, F. Yan, Y. Chen, S. Liu, M.-H. Yung, Y. Xu, and D. Yu, Superrobust Geometric Control of a Superconducting Circuit, *Phys. Rev. Appl.* **16**, 064003 (2021).
- [37] M.-Z. Ai, S. Li, R. He, Z.-Y. Xue, J.-M. Cui, Y.-F. Huang, C.-F. Li, and G.-C. Guo, Experimental realization of nonadiabatic holonomic single-qubit quantum gates with two dark paths in a trapped ion, *Fundamental Research* **2**, 661 (2022).
- [38] G. Feng, G. Xu, and G. Long, Experimental Realization of Nonadiabatic Holonomic Quantum Computation, *Phys. Rev. Lett.* **110**, 190501 (2013).
- [39] H. Li, Y. Liu, and G. Long, Experimental realization of single-shot nonadiabatic holonomic gates in nuclear spins, *Sci. China: Phys., Mech. Astron.* **60**, 1 (2017).
- [40] Z. Zhu, T. Chen, X. Yang, J. Bian, Z.-Y. Xue, and X. Peng, Single-Loop and Composite-Loop Realization of Nonadiabatic Holonomic Quantum Gates in a Decoherence-Free Subspace, *Phys. Rev. Appl.* **12**, 024024 (2019).
- [41] S. Arroyo-Camejo, A. Lazarev, S. W. Hell, and G. Balasubramanian, Room temperature high-fidelity holonomic single-qubit gate on a solid-state spin, *Nat. Commun.* **5**, 4870 (2014).
- [42] C. Zu, W.-B. Wang, L. He, W.-G. Zhang, C.-Y. Dai, F. Wang, and L.-M. Duan, Experimental realization of universal geometric quantum gates with solid-state spins, *Nature* **514**, 72 (2014).
- [43] B. B. Zhou, P. C. Jerger, V. O. Shkolnikov, F. J. Heremans, G. Burkard, and D. D. Awschalom, Holonomic Quantum Control by Coherent Optical Excitation in Diamond, *Phys. Rev. Lett.* **119**, 140503 (2017).
- [44] Y. Sekiguchi, N. Niikura, R. Kuroiwa, H. Kano, and H. Kosaka, Optical holonomic single quantum gates with a geometric spin under a zero field, *Nat. Photonics* **11**, 309 (2017).
- [45] N. Ishida, T. Nakamura, T. Tanaka, S. Mishima, H. Kano, R. Kuroiwa, Y. Sekiguchi, and H. Kosaka, Universal holonomic single quantum gates over a geometric spin with phase-modulated polarized light, *Opt. Lett.* **43**, 2380 (2018).
- [46] Y. Dong, S.-C. Zhang, Y. Zheng, H.-B. Lin, L.-K. Shan, X.-D. Chen, W. Zhu, G.-Z. Wang, G.-C. Guo, and F.-W. Sun, Experimental Implementation of Universal Holonomic Quantum Computation on Solid-State Spins with Optimal Control, *Phys. Rev. Appl.* **16**, 024060 (2021).
- [47] S.-B. Zheng, C.-P. Yang, and F. Nori, Comparison of the sensitivity to systematic errors between nonadiabatic non-Abelian geometric gates and their dynamical counterparts, *Phys. Rev. A* **93**, 032313 (2016).
- [48] J. Jing, C.-H. Lam, and L.-A. Wu, Non-Abelian holonomic transformation in the presence of classical noise, *Phys. Rev. A* **95**, 012334 (2017).
- [49] G. F. Xu, P. Z. Zhao, T. H. Xing, E. Sjöqvist, and D. M. Tong, Composite nonadiabatic holonomic quantum computation, *Phys. Rev. A* **95**, 032311 (2017).
- [50] G. F. Xu, D. M. Tong, and E. Sjöqvist, Path-shortening realizations of nonadiabatic holonomic gates, *Phys. Rev. A* **98**, 052315 (2018).
- [51] Y. Sekiguchi, Y. Komura, and H. Kosaka, Dynamical Decoupling of a Geometric Qubit, *Phys. Rev. Appl.* **12**, 051001 (2019).



- (2019).
- [52] P. Z. Zhao, X. Wu, and D. M. Tong, Dynamical-decoupling-protected nonadiabatic holonomic quantum computation, *Phys. Rev. A* **103**, 012205 (2021).
- [53] B.-J. Liu, X.-K. Song, Z.-Y. Xue, X. Wang, and M.-H. Yung, Plug-and-Play Approach to Nonadiabatic Geometric Quantum Gates, *Phys. Rev. Lett.* **123**, 100501 (2019).
- [54] F. Zhang, J. Zhang, P. Gao, and G. Long, Searching nonadiabatic holonomic quantum gates via an optimization algorithm, *Phys. Rev. A* **100**, 012329 (2019).
- [55] S. Li, T. Chen, and Z.-Y. Xue, Fast holonomic quantum computation on superconducting circuits with optimal control, *Adv. Quantum Technol.* **3**, 2000001 (2020).
- [56] T. Chen, P. Shen, and Z.-Y. Xue, Robust and Fast Holonomic Quantum Gates with Encoding on Superconducting Circuits, *Phys. Rev. Appl.* **14**, 034038 (2020).
- [57] S. Li and Z.-Y. Xue, Dynamically Corrected Nonadiabatic Holonomic Quantum Gates, *Phys. Rev. Appl.* **16**, 044005 (2021).
- [58] B.-J. Liu, Y.-S. Wang, and M.-H. Yung, Super-robust nonadiabatic geometric quantum control, *Phys. Rev. Res.* **3**, L032066 (2021).
- [59] Z.-C. He and Z.-Y. Xue, Robust nonadiabatic holonomic quantum gates on decoherence-protected qubits, *Appl. Phys. Lett.* **119** (2021), 10.1063/5.0063401.
- [60] K. Khodjasteh and L. Viola, Dynamically Error-Corrected Gates for Universal Quantum Computation, *Phys. Rev. Lett.* **102**, 080501 (2009).
- [61] X. Wang, L. S. Bishop, J. Kestner, E. Barnes, K. Sun, and S. Das Sarma, Composite pulses for robust universal control of singlet-triplet qubits, *Nat. Commun.* **3**, 997 (2012).
- [62] X. Rong, J. Geng, F. Shi, Y. Liu, K. Xu, W. Ma, F. Kong, Z. Jiang, Y. Wu, and J. Du, Experimental fault-tolerant universal quantum gates with solid-state spins under ambient conditions, *Nat. Commun.* **6**, 8748 (2015).
- [63] J. P. Kestner, X. Wang, L. S. Bishop, E. Barnes, and S. Das Sarma, Noise-Resistant Control for a Spin Qubit Array, *Phys. Rev. Lett.* **110**, 140502 (2013).
- [64] X. Wang, L. S. Bishop, E. Barnes, J. P. Kestner, and S. D. Sarma, Robust quantum gates for singlet-triplet spin qubits using composite pulses, *Phys. Rev. A* **89**, 022310 (2014).
- [65] P. Zanardi and M. Rasetti, Noiseless Quantum Codes, *Phys. Rev. Lett.* **79**, 3306 (1997).
- [66] L.-M. Duan and G.-C. Guo, Preserving Coherence in Quantum Computation by Pairing Quantum Bits, *Phys. Rev. Lett.* **79**, 1953 (1997).
- [67] D. A. Lidar, I. L. Chuang, and K. B. Whaley, Decoherence-Free Subspaces for Quantum Computation, *Phys. Rev. Lett.* **81**, 2594 (1998).
- [68] P. Krantz, M. Kjaergaard, F. Yan, T. P. Orlando, S. Gustavsson, and W. D. Oliver, A quantum engineer's guide to superconducting qubits, *Appl. Phys. Rev.* **6**, 021318 (2019).
- [69] M. Saffman, T. G. Walker, and K. Mølmer, Quantum information with Rydberg atoms, *Rev. Mod. Phys.* **82**, 2313 (2010).
- [70] X. Wang, Z. Sun, and Z. D. Wang, Operator fidelity susceptibility: An indicator of quantum criticality, *Phys. Rev. A* **79**, 012105 (2009).
- [71] J. Schwinger, Unitary operator bases, *Proc. Natl. Acad. Sci.* **46**, 570 (1960).
- [72] I. D. Ivonovic, Geometrical description of quantal state determination, *J. Phys. A: Math. Gen.* **14**, 3241 (1981).
- [73] A. Klappenecker and M. Rotteler, Mutually unbiased bases are complex projective 2-designs, *Proc. Int. Symp. Inf. Theory 2005*, 1740 (2005).
- [74] Z.-T. Liang, Y.-X. Du, W. Huang, Z.-Y. Xue, and H. Yan, Nonadiabatic holonomic quantum computation in decoherence-free subspaces with trapped ions, *Phys. Rev. A* **89**, 062312 (2014).
- [75] J. Zhou, W.-C. Yu, Y.-M. Gao, and Z.-Y. Xue, Cavity QED implementation of non-adiabatic holonomies for universal quantum gates in decoherence-free subspaces with nitrogen-vacancy centers, *Opt. Express* **23**, 14027 (2015).
- [76] Z.-Y. Xue, J. Zhou, and Z. D. Wang, Universal holonomic quantum gates in decoherence-free subspace on superconducting circuits, *Phys. Rev. A* **92**, 022320 (2015).
- [77] Z.-Y. Xue, J. Zhou, Y.-M. Chu, and Y. Hu, Nonadiabatic holonomic quantum computation with all-resonant control, *Phys. Rev. A* **94**, 022331 (2016).
- [78] D. M. Zajac, A. J. Sigillito, M. Russ, F. Borjans, J. M. Taylor, G. Burkard, and J. R. Petta, Resonantly driven CNOT gate for electron spins, *Science* **359**, 439 (2018).
- [79] T. Noh, G. Park, S.-G. Lee, W. Song, and Y. Chong, Construction of controlled-NOT gate based on microwave-activated phase (MAP) gate in two transmon system, *Sci. Rep.* **8**, 13598 (2018).
- [80] T. Xie, Z. Zhao, S. Xu, X. Kong, Z. Yang, M. Wang, Y. Wang, F. Shi, and J. Du, 99.92%-Fidelity CNOT Gates in Solids by Noise Filtering, *Phys. Rev. Lett.* **130**, 030601 (2023).